Quantitative Kinetic Model for Photoassembly of the Photosynthetic Water Oxidase from Its Inorganic Constituents: Requirements for Manganese and Calcium in the Kinetically Resolved Steps[†,‡]

Lyudmila Zaltsman, Gennady M. Ananyev, Edward Bruntrager, and G. Charles Dismukes*

Hoyt Laboratory, Department of Chemistry, Princeton University, Princeton, New Jersey 08544

Received January 27, 1997; Revised Manuscript Received May 13, 1997[⊗]

ABSTRACT: The process of photoactivation, the assembly of a functional water-oxidizing complex (WOC) from the apoproteins of photosystem II of higher plants and inorganic cofactors (Mn^{2+}, Ca^{2+}, and Cl^-), was known from earlier works to be a two-step kinetic process, requiring two light-induced processes separated by a slower dark period. However, these steps had not been directly resolved in any kinetic experiment, until development of an ultrasensitive polarographic O_2 electrode and synthesis of an improved chelator for cofactor removal allowed direct kinetic resolution of the first pre-steady state intermediate [Ananyev, G. M. & Dismukes, G. C. (1996a) *Biochemistry 35*, 4102−4109]. Herein, the dependence of the rates of each of the first two light steps and the dark step of photoactivation was directly determined in spinach PSII membranes over a range of calcium and manganese concentrations at least 10-fold lower than those possible using commercial O_2 electrodes. The following results were obtained. (1) One Mn^{2+} ion binds and is photooxidized to Mn^{3+} at a high-affinity site, forming the first light-induced intermediate, IM_1. Formation of IM_1 is coupled to the dissociation of a bound Ca^{2+} ion either located in the Mn site or coupled to it. (2) The inhibition constant for Ca^{2+} dissociation from this site is equal to 1.5 mM. (3) The dissociation constant of Mn^{2+} at this high-affinity site is equal to 8 μM at the optimum calcium concentration for O_2-evolving activity of 8 mM, in agreement with the high-affinity site for electron donation to PSII. (4) Prior to the next photolytic step, one Ca^{2+} ion must bind at its effector site so that stable photooxidation of a second Mn^{2+} ion can occur, forming the second light-induced intermediate, IM_2. This dark process is the rate-determining step. (5) The Michaelis constant for recovery of O_2 evolution by Ca^{2+} binding at this effector site (K_m) is equal to 1.4 mM, a value that is the same as that measured for the calcium requirement for O_2 evolution in intact PSII. (6) The low quantum yield for the formation of IM_2 from IM_1 increases linearly with the duration of the dark period up to the longest period we could examine (10 s). Accordingly, the rate limitation in the second photolytic step originates from a slow calcium-induced dark rearrangement of the first intermediate, IM_1, which we propose to be a protein conformational change that allows stable binding of the next Mn^{2+} ion. We further propose that the single Ca^{2+} ion which is required for assembly of the Mn_4 cluster is equivalent to the Ca^{2+} ion which functions at the "gatekeeper" site in intact O_2-evolving centers, where it plays a role in limiting substrate access to the Mn_4 cluster [Sivaraja, M., et al. (1989) *Biochemistry 28*, 9459−9464; Tso, J., et al., (1991) *Biochemistry 30*, 4734−4739]. A molecular model for photoactivation is proposed and discussed.

Photoactivation is the process of binding and photooxidation of the inorganic cofactors (manganese, calcium, and chloride) within the apoprotein components of photosystem II of green plants and cyanobacteria. This is an activated process which requires light and produces a functional water-oxidizing complex. Photoactivation occurs *in vivo* during normal daily variations in light/dark periods to a greater or lesser extent depending on the organism and environmental stresses (Callahan et al., 1986; Jegerschold & Styring, 1989). It also occurs during normal growth of plants and following the replacement of PSII[1] proteins irreversibly damaged by light, in the process of photoinhibition (Anderson, 1988; Vasilikiotis & Melis, 1994). The process of photoinhibition has been linked to aberrant photochemistry stemming from defective photoactivation within either the water-oxidizing complex (WOC), the PSII reaction center, or both (Yamashita & Ashizawa, 1983; Powels, 1984; Aro et al., 1993). The ability to bind and photooxidize manganese ions and other electron donors at the WOC during photoactivation helps to protect PSII protein components from donor-side destruction (Theg et al., 1986; Klimov et al., 1990a,b).

[†] This work was supported by the National Institutes of Health (Grant GM39932).

[‡] Dedicated to Professor George Cheniae on the occasion of his 70th birthday.

* To whom correspondence should be addressed. Fax: (609) 258-1980. E-mail: dismukes@chemvax.princeton.edu.

[⊗] Abstract published in *Advance ACS Abstracts,* July 1, 1997.

[1] Abbreviations: Chl, chlorophyll; DCBQ, 2,5-dichloro-*p*-benzoquinone; EPR, electron paramagnetic resonance; LED, light-emitted diode; MES, 2-(*N*-morpholino)ethanesulfonic acid; P680, primary electron donor; PSII, photosystem II; Pheo, primary pheophytine electron acceptor of PSII; Q_A and Q_B, primary and secondary plastoquinone electron acceptors, respectively; RC, reaction center; $t_{1/2}$, half-time kinetics of pulsed light photoactivation of oxygen evolution; TPDBA, *N,N,N′,N′*-tetrapropionato-1,3-bis(aminomethyl)benzene; Y_{ss}, steady state level kinetics of pulsed light photoactivation of oxygen evolution; Y_z, redox-active tyrosine-161 of the D1 polypeptide; WOC, water-oxidizing complex.

S0006-2960(97)00187-6 CCC: $14.00

Photoactivation has also been studied *in vitro* in considerable detail and used to characterize the inorganic composition of the WOC (Cheniae & Martin, 1966, 1971). It occurs in isolated chloroplasts (Yamashita & Tomita, 1974; Ono & Inoue, 1983a,b) and isolated PSII membranes (Tamura & Cheniae, 1987; Tamura et al., 1989; Miyao & Inoue, 1991; Ananyev & Dismukes, 1996a,b). Numerous works have been devoted to the elucidation of the mechanism of photoactivation by studying the time course of the recovery of O_2 evolution under continuous and intermittent light (Tamura & Cheniae, 1987; Miller & Brudvig, 1989; Tamura et al., 1991; Blubaugh & Cheniae, 1992). These kinetic studies had to be performed at concentrations of Mn^{2+} at least 10 times above the PSII reaction center concentration due to sensitivity limitations of the oxygen detection methods. On the basis of such studies using intermittent light, Cheniae's group found clear evidence for a two-quantum model for photoactivation, where two Mn^{2+} ions sequentially bind to the apo-PSII complex and are photooxidized. Completion of photoactivation was proposed to require binding of two additional Mn^{2+} ions with subsequent photooxidation producing a stable WOC. Binding of the second Mn^{2+} ion was proposed to be the overall rate-determining step of photoactivation. This model was further supported by Miller and Brudvig (1989, 1990), who also showed by EPR that the first light-induced intermediate of photoactivation resulted in the disappearance of Mn^{2+} from solution. They hypothesized on the basis of their kinetic studies that a second intermediate could contain a dimanganese $Mn^{2+}Mn^{3+}$ center which, although undetected, could be photooxidized in the next light-dependent step to yield $Mn^{3+}Mn^{3+}$.

The presence of a dark step between the light steps in photoactivation was first suggested on the basis of the requirement for a dark interval between light flashes for optimization of the quantum yield for photoactivation (Tamura & Cheniae, 1987; Miyao & Inoue, 1991; Tamura et al., 1991). The half-time for the decay of this intermediate was estimated to be 1−1.5 s (Tamura & Cheniae, 1987).

The first direct kinetic resolution of a pre-steady state intermediate became possible due to an advance in oxygen detection sensitivity and response time, as well as development of a gentler and more reproducible method for complete extraction of the inorganic cofactors. These improvements allowed monitoring of the photoactivation kinetics in the presence of 10−100-fold lower concentrations of Mn^{2+} (Ananyev & Dismukes, 1996a,b). Under such conditions, the kinetics of O_2 evolution recovery in the presence of substoichiometric or near-stoichiometric concentrations of Mn^{2+} were found to follow a biphasic behavior, with a clear lag phase preceding an exponential recovery phase. The exponential recovery process was shown to involve binding of one Mn^{2+} ion in the second (rate-determining) step of photoactivation.

Extensive studies have attempted to elucidate the role of Ca^{2+} in photoactivation, but the function of this cofactor in assembly and activity is still uncertain. On the one hand, the binding of one Ca^{2+} ion is required for oxygen evolution in the functional WOC [for reviews, see Yocum (1991), Debus (1992), Andreasson et al. (1995), and Han & Katoh (1995)]; therefore, Ca^{2+} must bind to PSII at some stage of photoactivation. On the other hand, whether binding of Ca^{2+} is essential for the assembly of the tetramanganese cluster remains a controversial issue. Ono and Inoue (1983a,b) proposed on the basis of the studies of photoactivation in the presence of an ionophore for divalent cations that both Mn^{2+} and Ca^{2+} should be bound to their specific sites in order for photoactivation to occur, although no direct evidence was available. However, according to other works performed at high Mn^{2+} concentrations, Ca^{2+} is not required for the assembly of the tetramanganese cluster, but only for the expression of oxygen evolution (Miller & Brudvig, 1989; Tamura et al., 1989). In the recent work by Ananyev and Dismukes (1966a,b), it was directly demonstrated that, when near-stoichiometric concentrations of Mn^{2+} are used to eliminate interference at other sites, preassembly of an intermediate prior to an active cluster requires the presence of Ca^{2+}. However, in this work, it was not shown which particular step(s) of photoactivation require Ca^{2+} binding.

Several roles were suggested regarding the possible role of Ca^{2+} in photoactivation, including stabilization of photoactivation intermediates (Miller & Brudvig, 1989), or in facilitating conformational changes accompanying the rate-determining step (Chen et al., 1995). However, no direct support for either of these roles was provided. It was also shown that in the presence of high concentrations of Mn^{2+} in the medium Ca^{2+} prevents binding and photooxidation of nonspecific (excess) manganese ions, which diminish the yield of active centers (Chen et al., 1995). However, the most recent work from Cheniae's group claims that calcium is not essential for the assembly of the tetramanganese cluster, but instead is required for a subsequent conformational activation of the tetramanganese cluster or PSII protein (Chen et al., 1995). Besides being an essential inorganic cofactor for photoactivation and oxygen evolution, Ca^{2+} was also shown to slow the overall rate of photoactivation by competing with Mn^{2+} for its binding site(s) (Ono & Inoue, 1983a,b; Hsu et al., 1987; Tamura & Cheniae, 1987; Miller & Brudvig, 1989).

In the present paper, the kinetic properties of the first photoactivation intermediate directly resolved in our earlier work are studied in further detail (Ananyev & Dismukes, 1996a,b). The rate constants for both of the elementary photolytic steps of photoactivation are determined, as well as the molecularities of Ca^{2+} and Mn^{2+} in each step. We present direct kinetic evidence demonstrating the essential ligation of Ca^{2+} in a dark step following photooxidation of the first Mn^{2+} ion. The low quantum yield for photoactivation is measured and shown to be directly limited by this dark calcium-induced process. Finally, we propose a molecular model for the first two steps in photoactivation.

MATERIALS AND METHODS

PSII-enriched membrane fragments were prepared from market spinach using the method of Berthold et al. (1981) with some minor modifications (Ghanotakis et al., 1984). The samples (2 mg of Chl/mL) were frozen with 10% glycerol in liquid nitrogen and stored at −196 °C until they were slowly thawed and washed once in the medium containing 300 mM sucrose, 35 mM NaCl, and 50 mM MES/NaOH buffer at pH 6.2 (standard assay medium). The oxygen evolution rate under continuous illumination (V_{O_2}) of the untreated PSII membrane fragments with 0.8 mM K_3FeCN_6/1.2 mM DCBQ as electron acceptors was 400−500 μmol of O_2 (mg of Chl)$^{-1}$ h^{-1}. The concentration of the

PSII reaction center was measured from the photoinduced absorption changes of Pheo at 685 nm using the extinction coefficient ϵ of 0.32×10^5 M^{-1} cm^{-1} (Klimov et al., 1982).

Manganese and calcium were removed from PSII membranes (0.5 mg of Chl/mL) using the standard assay medium in the presence of 35 mM TPDBA and 1 mM ascorbate (Ananyev & Dismukes, 1996a,b). Photoactivation and polarographic detection of O_2 were performed directly in a home-built microcell as described earlier (Ananyev & Dismukes, 1996a,b). The cell characteristics include a 5 μL active sample volume, a 100 msec time constant, and a sensitivity of 50 fmol of O_2. The current signal from the cell was amplified in a two-stage band-pass-filtered amplifier and sent to an analog-to-digital converter and computer for accumulation and processing [WINDAQ Data Acquisition System (DATAQ Instruments, Inc.)]. The cell was illuminated by an ultrabright LED with a wavelength maximum of 660 nm and an I_p of 800 mW/cm^2 (HLMP-8102, Hewlett-Packard), allowing for the flash illumination in the range 0.001 s to ∞ (continuous). In the present work, the pulsed light parameters were as follows, unless otherwise indicated. The duration of the light pulses (t_{light}) was equal to 40 ms, and the duration of the dark period between flashes (t_{dark}) was equal to 3 s. These conditions were found to optimize the yield of photoactivation in our earlier work (Ananyev & Dismukes, 1996a). All experiments were conducted in the standard assay medium containing 1 μM apo-PSII RC, 0.8 mM $K_3Fe(CN)_6$ as an electron acceptor, as well as $MnCl_2$, $CaCl_2$, and other salts at the concentrations indicated in the text or figure legends.

Electron transport measurements were performed in the same home-built cell modified to measure the redox potential of the electrochemical couple $K_3Fe(CN)_6/K_4Fe(CN)_6$. The following changes were made to achieve this purpose. (1) The oxygen-permeable silicone membrane was removed, and (2) the platinum/iridium electrode worked as a probe of the redox potential of the medium by allowing it to float at the potential of the medium.

The error associated with measurements of peak heights from data similar to those depicted in Figure 1, ultimately leading to determination of all rate constants, is ignorable in comparison to the random variation between samples. The estimated error in rate constants associated with the measurements of the rate constant for the rate-determining step (k_2) from measurements performed on the same day on the same sample is equal to $\sim\pm3\%$. The absolute values of rate constants measured on different samples can vary significantly, depending on the quality of biochemical preparations, the age of the PSII membranes, and the amount and duration of exposure to the chelator used for extraction. When these factors were controlled, the observed trends in the dependencies depicted on all plots were found not to vary from sample to sample. All derived quantities were determined at least twice under identical conditions. In the graphical and numeric treatment of experimental data, we used two software packages: Cricket Graph 1.3 for Macintosh (Cricket Software) and Matlab 4.2c for UNIX (The MathWorks, Inc.).

RESULTS

Kinetics of Photoactivation and Electron Transport of Apo-PSII Membranes. Figure 1A,B demonstrates a typical time course for recovery of O_2 evolution in the presence of

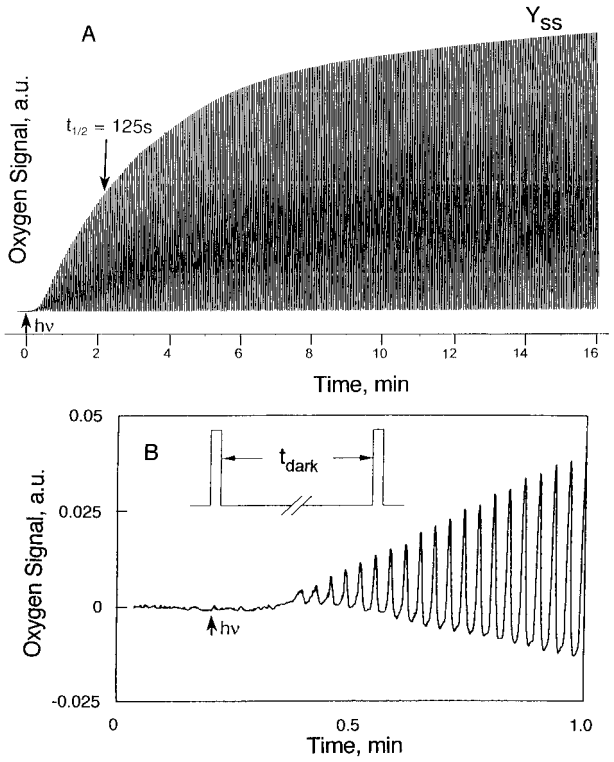

FIGURE 1: Typical kinetics of the rate of oxygen evolution recovery by photoactivation in TPDBA-extracted BBY PSII membranes using light pulses from an LED illumination source (t_{light} = 30 ms, t_{dark} = 3 s) in the presence of 8 μM $MnCl_2$ and 8 mM $CaCl_2$. (A) The full time course of photoactivation with 320 light pulses over 16 min. A baseline has been subtracted. (B) Repeat of the same experiment except using a higher time resolution over the initial minute. The inset shows the pattern of pulsed light illumination.

an 8-fold excess of $MnCl_2$ (8 μM) and sufficient $CaCl_2$ to saturate the yield of photoactivatable centers (8 mM). The yield of O_2 evolution is zero during the first several flashes and then rises exponentially until it reaches a steady state level after approximately 220 light pulses over 11 min of illumination. The duration of the initial delay in O_2 production varies between 3 and 25 flashes, depending on the concentration of the inorganic cofactors, the age of the PSII membranes, and the duration of the exposure to the chelator TPDBA. Hence, comparison between samples was always made using the same preparation and treatment. Figure 2 shows a semilogarithmic plot of the fraction of the inactive (but photoactivatable) centers *vs* total time of pulsed light illumination. This form of presentation of the data clearly demonstrates that the recovery of O_2 evolution is a biphasic process and that the second step obeys a single-exponential process.

In order to test the possibility that the delay in oxygen evolution (lag phase) could be due to limitations in the electron transport capacity of apo-PSII during the initial stage of illumination, we measured the rate of electron transfer to ferricyanide in the same cell and under illumination and sample conditions identical to those used for photoactivation. Unlike O_2 production, the rate of ferricyanide reduction, shown in Figure 3, is high initially and falls by $\sim$30% after 12 flashes to a slower rate of decay. This high initial rate demonstrates that the lag phase in O_2 production is not caused by limitations of the electron transport chain. The rate of ferricyanide reduction depends on the Mn^{2+} concentration (not shown) and so results from photooxidation of Mn^{2+}

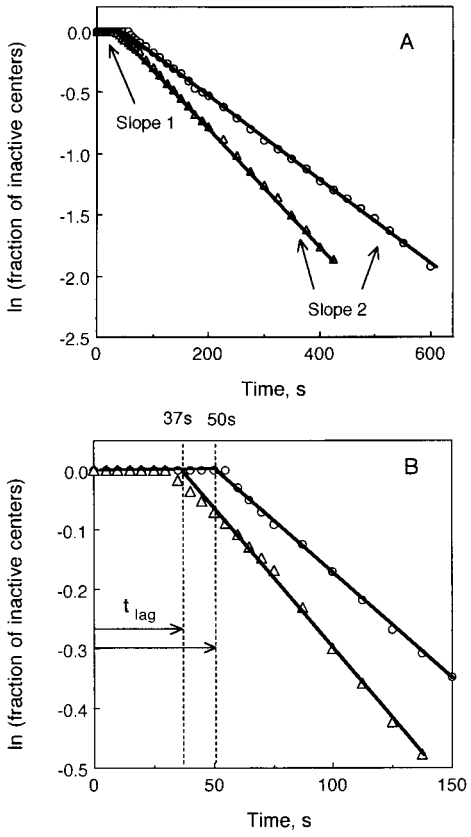

FIGURE 2: (A) Semilogarithmic plots of the fraction of inactive centers *vs* pulsed light illumination time for two Mn^{2+} concentrations equal to 2 μM (○) and 4 μM (△) in the presence of 8 mM Ca^{2+}. (B) The initial part of panel A, corresponding to the first 150 s of illumination.

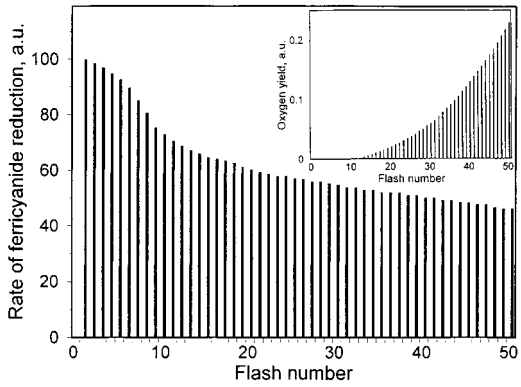

FIGURE 3: Dependence of the rate of the flash-induced reduction of ferricyanide to ferrocyanide on the duration of pulsed light illumination during the initial stage of photoactivation in the presence of 8 μM $MnCl_2$ and 8 mM $CaCl_2$. The inset shows the dependence of the flash oxygen yield on the duration of pulsed light illumination for the same sample.

during assembly of clusters which go on to form active O_2-producing Mn_4 clusters.

The 30% drop in the initial rate of electron transport after 12 flashes correlates approximately with the disappearance of the lag phase in O_2 production when measured under identical conditions using the Clark cell configuration described in Materials and Methods. For comparison, a photoactivation trace showing the recovery of O_2 evolution is plotted in Figure 3 (inset). As shown earlier, the kinetics and the yield of photoactivation do not change with ferricyanide concentration in the range of 0.3−1.0 mM. Therefore, the drop in the rate of ferricyanide reduction is not due

Scheme 1: Model of Photoactivation Based on Directly Observed Kinetic Features

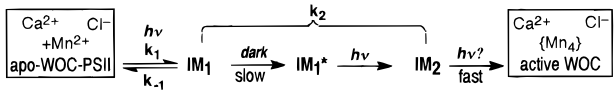

to a change in the electrochemical potential of the medium as ferricyanide is consumed (Ananyev & Dismukes, 1996a). The correlation in rates shown in Figure 3 suggests that the drop in the rate of ferricyanide reduction is likely due to a slower rate of electron donation from the first intermediate, i.e. from photooxidation of the second Mn^{2+} ion compared to the first Mn^{2+} ion.

As shown later, we know that the lag phase seen in Figure 3 (inset) corresponds to the photooxidation of the first Mn^{2+} ion. Hence, the relative rates for electron donation from Mn^{2+} reacting with Tyr Z (Y_z^+) in the first photooxidized intermediate, IM_1^+, *vs* Y_z^+ in the photooxidized apo-PSII can be estimated from the relative slopes of the ferricyanide reduction kinetics. Inspection of Figure 3 reveals that the initial Mn^{2+} is photooxidized roughly 5 times more effectively than the second Mn^{2+} in the rate-limiting step of photoactivation. We have not examined if this slower electron donation rate for the second Mn^{2+} ion is due to weaker binding (i.e. partial occupation), a slower binding rate of the second Mn^{2+} ion, or an intrinsically lower electron transfer rate from a fully occupied second Mn^{2+} site.

Minimal Kinetic Model for Photoactivation. The initial lag phase in the kinetics was attributed in our earlier work to the accumulation of a pre-steady state intermediate (the process described by slope 1 in Figure 2A and the first step in Scheme 1) (Ananyev & Dismukes, 1996a). After this lag, a steady state rate is achieved, and the overall rate of photoactivation is determined by the slow conversion of the first intermediate to the second intermediate. This process is described by slope 2 in Figure 2A and the second step in Scheme 1. The subsequent steps of photoactivation, generating a functional WOC, occur fast and are kinetically indistinguishable. These considerations, as well as earlier works (Tamura & Cheniae, 1987), lead to the minimal model of photoactivation illustrated in Scheme 1. The requirement for a dark interval between the light flashes (t_{dark}) is essential for the optimization of the quantum yield of photoactivation (Tamura & Cheniae, 1987; Klimov et al., 1990; Ananyev & Dismukes, 1996a,b). This step is depicted in Scheme 1 as the second event following the initial photooxidation step. Although there may be more than one dark step required for photoactivation, only steps preceding the rate-limiting step influence the kinetics of photoactivation.

Determination of Rate Constants in the Minimal Model of Photoactivation. Below, we will summarize an approach for determination of three essential rate constants (k_1, k_{-1}, and k_2) noted in Scheme 1. The numerical values at fixed cofactor concentrations are listed in Table 1. The molecularities in Mn^{2+} and Ca^{2+} for each elementary reaction will be determined from the dependencies of k_1, k_{-1}, and k_2 on the Mn^{2+} and Ca^{2+} concentrations. The dependence of kinetics on the apo-PSII concentration was examined in the range of 0.5−2 μM RC and found to be first-order. It was found that at the different RC concentrations but at the same relative concentrations of Mn^{2+} per RC the kinetics of photoactivation are the same (data not shown).

Table 1: Estimates of the Apparent Rate Constants and Binding Constants for Mn^{2+} and Ca^{2+} in the First Two Kinetically Resolved Steps of Photoactivation

Apparent Rate Constants[a]		
k_1 (s^{-1})	k_{-1} (s^{-1})	k_2 (s^{-1})
0.080	0.063	0.0058
Apparent Dissociation Constants[b]		
K_{Mn} (μM) in the first Mn site	$K_{m\,Ca}$ (mM) in the rate-determining step	$K_{i\,Ca}$ (mM) in the first Mn site
8	1.4	1.5

[a] All rate constants are determined for 10 μM Mn^{2+} and 8 mM Ca^{2+}. [b] The dissociation constant for Mn was determined at 8 mM Ca^{2+}, and the dissocation constants for Ca^{2+} are determined at 10 μM Mn^{2+} from the kinetics of photoactivation as described in the text.

From the data given in Figure 2, the rate constant for the rate-determining step of photoactivation, k_2, was obtained from the negative slope of the semilogarithmic plot of the fraction of the inactive centers *vs* time in the interval starting immediately after the break point and followed for at least 80−90% of the recovery. The result is listed in Table 1. All plots give straight lines with correlation coefficients of ≥ 0.97, indicating that a single-exponential process governs the recovery of O_2 evolution activity. This result offers an important insight into the mechanism, considering that at the stoichiometric or near-stoichiometric concentrations of Mn^{2+} used in our studies there is considerable depletion of free Mn^{2+} and apo-PSII during photoactivation. In order for a single-exponential rate law to emerge from an intrinsically bimolecular rate process such as this, the quantum yield for the second photolytic process must be rate-limited by an intrinsic unimolecular process. We show later that this unimolecular process corresponds to the dark step.

Direct experimental determination of k_{-1}, decay of IM_1, was carried out by the procedure illustrated in Figure 4A. The usual pattern of pulse light illumination was interrupted by a continuous dark period of variable duration. The dark period was started after 25−50 s of pulsed light illumination at the end of the lag phase, as determined from the break point in Figure 2. At this time, the yield of IM_1 is maximal relative to IM_2, and no significant amount of IM_2 has formed. The kinetics of dark decay of IM_1 were measured from the duration of the subsequent recovery of the lag phase after the dark period (symbolized as t_{decay}). A typical plot of t_{decay} *vs* duration of the dark period is shown in Figure 4B. t_{decay} gradually increases with increasing dark period until it reaches a plateau equal to the duration of the lag phase in the experiment where no dark period was given. The time for dark decay of 50% of the first intermediate was determined directly from the plot of t_{decay} *vs* dark period, as indicated in Figure 4B. In the model of unimolecular decay, the value of k_{-1} was calculated with $k_{-1} = \ln 2/t_{1/2}$. The result is listed in Table 1.

When the values of k_{-1} and k_2 are known at fixed concentrations of Mn^{2+} and Ca^{2+}, the value of k_1 is fixed by the model in Scheme 1. The general kinetic solution to Scheme 1 yields the solution for $[IM_1]$ expressed in terms of the rate constants k_1, k_{-1}, and k_2 (Connors, 1990). Assuming that the end of the lag phase corresponds to a time when the concentration of IM_1 reaches its steady state and hence $d[IM_1]/dt = 0$, the lag time can be expressed in terms of three rate constants as

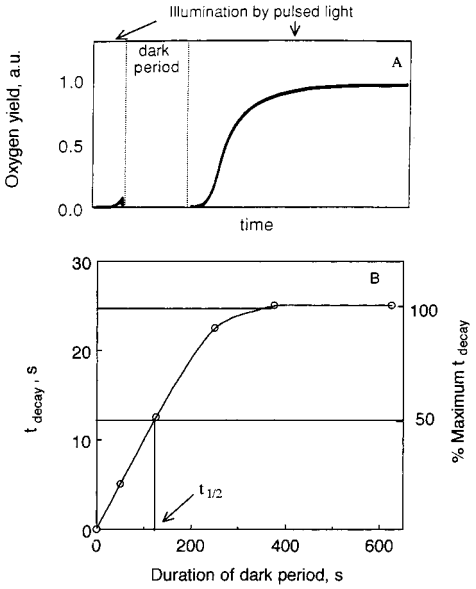

FIGURE 4: (A) Scheme for the experimental determination of k_{-1}. The solid line shows a typical time course of recovery of oxygen evolution as a function of the total time of pulsed light illumination before and after a continuous dark period is given. (B) Dependence of t_{decay} on the duration of the dark period in the presence of 10 μM $MnCl_2$ and 1 mM $CaCl_2$. t_{decay} was determined at the break point in the semilogarithmic plots of the fraction of inactive centers *vs* time, as depicted in Figure 2B.

$$t_{lag} = \frac{\ln[(k_1+k_1+k_2)^2/4k_1k_2]}{[(k_1 + k_1 + k_2)^2 - 4k_1k_2]^{1/2}} \qquad (1)$$

The duration of the lag phase in our experiments was determined from the break point in the plots similar to Figure 2, i.e. when the rate-limiting step is extrapolated to 100% inactive centers.

Dependence of k_2 onManganese and Calcium Concentrations. Involvement of Mn^{2+} in the rate-determining step of photoactivation was examined in our earlier work (Ananyev & Dismukes, 1996a). We previously determined that 1.1−1.2 atoms of Mn^{2+} are photooxidized in the second light-induced step of photoactivation.

The dependence of k_2 on the Ca^{2+} concentration was measured from 1 to 60 mM at a fixed Mn^{2+} concentration (10 μM) as depicted in Figure 5. The graph shows two different phases: stimulation of k_2 at low Ca^{2+} concentrations (up to 8 mM) and inhibition of k_2 at higher concentrations. The strong stimulatory effect of Ca^{2+} is evidence for the ligation of Ca^{2+} in the second step of photoactivation. From Figure 5, the Michaelis constant, K_m, for Ca^{2+} stimulation of k_2 was measured to be 1.4 mM, as the concentration corresponding to 50% of the maximal k_2. Analysis of the initial slope of Figure 5 gives an estimation for the molecularity of the second step in Ca^{2+}, equal to approximately 1.

In order to elucidate the nature of the inhibitory effect of Ca^{2+} at concentrations above 8 mM, k_2 was measured as a function of the concentration of nonessential cations like Mg^{2+} or Na^+ in the photoactivation medium (containing 8 mM Ca^{2+} and 10 μM Mn^{2+}). According to inset in Figure 5, the inhibition of k_2 *vs* cationic strength of the solutions is practically the same for both Ca^{2+} and Mg^{2+}, while the effect of Na^+ is somewhat weaker. These data show that the inhibitory effect of cations, including Ca^{2+}, at high concentrations is nonspecific, suggesting electrostatic screening of

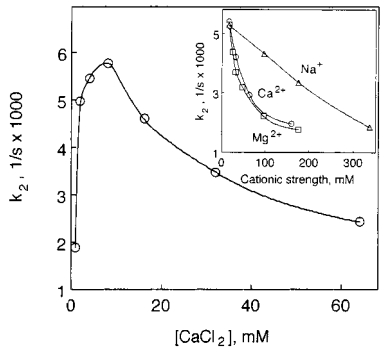

FIGURE 5: Dependence of the rate constant for the second photolytic step of photoactivation (k_2) on the $CaCl_2$ concentration in the presence of 8 μM $MnCl_2$. The inset shows the effect of the cationic strength of the solution, defined as $1/2(4[Ca^{2+}] + n^2[Me^{n+}])$, on k_2 in the presence of 10 μM $MnCl_2$, 8 mM $CaCl_2$, and additional $CaCl_2$ (circles), $MgCl_2$ (squares), or NaCl (triangles). Only cationic strength due to Ca^{2+}, Mg^{2+}, and Na^+ is considered.

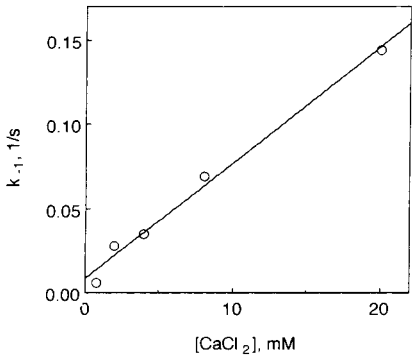

FIGURE 6: Dependence of the rate constant for decay of the first intermediate (k_{-1}) on the $CaCl_2$ concentration in the presence of 10 μM $MnCl_2$.

Mn^{2+} binding or possibly an electrostatically induced unfavorable change in the protein conformation.

Dependence of k_{-1} on Manganese and Calcium Concentrations. Figure 6 shows the dependence of k_{-1} on Ca^{2+} concentration, measured as previously described. The graph yields a straight line with a rate constant of zero at $[Ca^{2+}] = 0$. A graph of $\ln(k_{-1})$ *vs* $\ln[Ca^{2+}]$ (not shown) gives a straight line with a slope equal to 1.0, indicating that the process is first-order in the Ca^{2+} concentration. The data show that the dark decay of the first intermediate for reforming the initial state involves rebinding of one Ca^{2+} atom.

The light-induced initial step (k_1 process) involves binding of one manganese atom, as we show below. Therefore, the dark decay of the first intermediate described by the rate constant k_{-1} should represent dissociation of this manganese atom, if there are no intermediates between IM_1 and the initial state. If this unimolecular decay model is correct, the rate constant k_{-1} should be independent of Mn^{2+} ion concentration. At low Mn^{2+} concentrations, where competition with the essential Ca^{2+} binding site required for O_2 activity should be negligible, this prediction of the model has been tested experimentally at a fixed $[Ca^{2+}]$ of 8 mM and three concentrations of Mn^{2+} (4, 10, and 20 μM). The values of k_{-1} were in fact found to be the same for all these Mn^{2+} concentrations. That means that free Mn^{2+} is not required for reduction and release of bound Mn^{3+} during decay of IM_1.

Dependence of k_1 on Manganese and Calcium Concentrations. The dependence of the initial light-induced step on

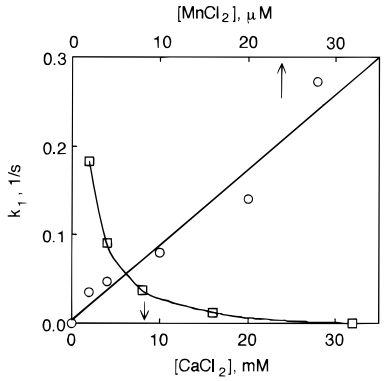

FIGURE 7: Dependence of the rate constant for the first step in photoactivation (k_1) on concentrations of the essential cofactors. The dependence of k_1 on the $MnCl_2$ concentration in the presence of 8 mM $CaCl_2$ (circles) is shown on the upper axes. The dependence of k_1 on the $CaCl_2$ concentration in the presence of 8 μM $MnCl_2$ (squares) is shown on the lower axes.

Mn^{2+} concentration is illustrated in Figure 7. The molecularity of the reaction in Mn^{2+} could be determined over a limited range (2−30 μM) from the plot of $\ln(k_1)$ *vs* $\ln[Mn^{2+}]$. The graph is a straight line with the slope of 0.9, establishing that binding of one Mn^{2+} atom occurs during the first step of photoactivation.

The dependence of k_1 on Ca^{2+} concentration at a fixed $[Mn^{2+}]$ of 8 μM shows that Ca^{2+} slows the rate of the first step of photoactivation (Figure 7). The graph represents a typical plot of competitive inhibition of the Mn^{2+} binding site by Ca^{2+}. Standard analysis yields the inhibition constant (K_i) for Ca^{2+} at the Mn^{2+} site according to the formula

$$[I]_{0.5} = \left(1 + \frac{[Mn^{2+}]}{K_{Mn}}\right)K_i \qquad (2)$$

where $[I]_{0.5}$ is the inhibitor concentration required for 50% inhibition (Segel, 1975). The value of k_1 in the absence of the inhibitor was approximated to be 0.28 s^{-1} by extrapolating the initial portion of the plot to $[Ca^{2+}] = 0$. Thus, 50% inhibition occurs when $k_1 = 0.14$ s^{-1} and $[Ca^{2+}] = 3$ mM. When $K_{Mn} = 8$ μM (calculated below), the K_i for Ca^{2+} at the first Mn^{2+} binding site is found to be 1.5 mM.

Determination of the Dissociation Constant for Manganese. The apparent dissociation constant for manganese (Mn^{2+}/Mn^{3+}) at the first manganese binding site (K_{Mn}) can be extracted from the following equations:

$$\text{apo-PSII} + Mn^{2+} \underset{k_{-1}}{\overset{k_1'}{\rightleftharpoons}} IM_1$$

$$k_1' = \frac{k_1}{[Mn^{2+}]} \quad K_{Mn} = \frac{k_{-1}}{k_1}[Mn^{2+}] \qquad (3)$$

This equation is not an elementary binding step as it involves binding and photooxidation of Mn^{2+} and dissociation of Mn^{3+}, or the reduction of Mn^{3+} followed by dissociation. In this equation, $[Mn^{2+}]$ represents the concentration of free Mn^{2+}. In order to determine K_{Mn}, we substituted for k_1 in eq 3 the linear plot in Figure 7 for the dependence of k_1 on $[Mn^{2+}]$ and extrapolated to the limiting condition of $[Mn^{2+}] \rightarrow \infty$, which allows us to ignore the small fraction of bound Mn^{2+}. The value of k_{-1} was obtained from Figure 6 at the same concentration of Ca^{2+} (8 mM) as that used for

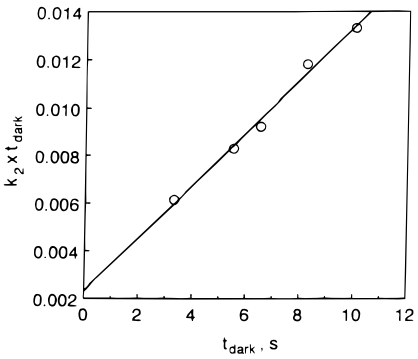

FIGURE 8: Dependence of the product k_2t_{dark} on t_{dark}, the dark interval between light flashes, at 4 mM $CaCl_2$ and 10 μM $MnCl_2$.

determination of k_1. From this analysis, K_{Mn} was found to be 8 μM at the optimal Ca^{2+} concentration for O_2 evolution activity (Table 1). This value of K_{Mn} is in agreement with the apparent dissociation constant of photooxidized manganese at the high-affinity site, estimated previously (Hoganson et al., 1989; Blubaugh & Cheniae, 1990).

Dependence of k_2 on the Duration of the Dark Interval between Light Flashes. The value of k_2 was determined as a function of the duration of the dark interval between flashes (t_{dark}, inset in Figure 1B). Since the k_2 step is a combination of dark- and light-driven steps, as shown in Scheme 1, the light step cannot occur until the dark step preceding it is completed. So, the value of k_2t_{dark} is a measure of the quantum efficiency of the rate-determining step of photoactivation. Figure 8 shows that the value of quantum efficiency of the rate-determining step steadily increases in the range of dark intervals between 3 and 10 s. These results demonstrate that the duration of the dark interval required for increasing the probability of the second photooxidation step is longer than 10 s, the longest interval we could measure reliably in our cell. Numerically, the quantum yield utilizing a 10 s dark interval is equal to $\sim 10^{-4}$ ($Mn^{2+} \rightarrow Mn^{3+}$ per photon absorbed) at a concentration of Mn^{2+} equal to 10 μM and a [Ca^{2+}] of 4 mM.

DISCUSSION

In the present work, we found kinetic parameters for photoactivation of the WOC over a range of concentrations of manganese which covers substoichiometric and greater levels. The results could be interpreted with a simplified kinetic model based on direct kinetic resolution of a pre-steady state intermediate. We found that one Mn^{2+} ion binds and is photooxidized in each of the first two photolytic steps of photoactivation. In order for the second photolytic step to occur, one Ca^{2+} ion must bind during an intervening slow dark step and is responsible for limiting the quantum yield of the overall process.

The sequential binding and photooxidation of two Mn^{2+} ions in two successive steps during assembly of the tetramanganese cluster of the WOC is in agreement with the two-quantum model proposed earlier by Tamura and Cheniae (1987). The value of the half-time for the experimentally determined exponential phase is in the range of 2−7 min, depending upon cofactor concentrations, which is also in agreement with the result of 6 min estimated by Tamura & Cheniae (1987). This time corresponds to a mean lifetime for two competing reactions affecting the concentration of IM_1: the dark rearrangement of IM_1 in the presence of

Scheme 2: Molecular Model of Photoactivation[a]

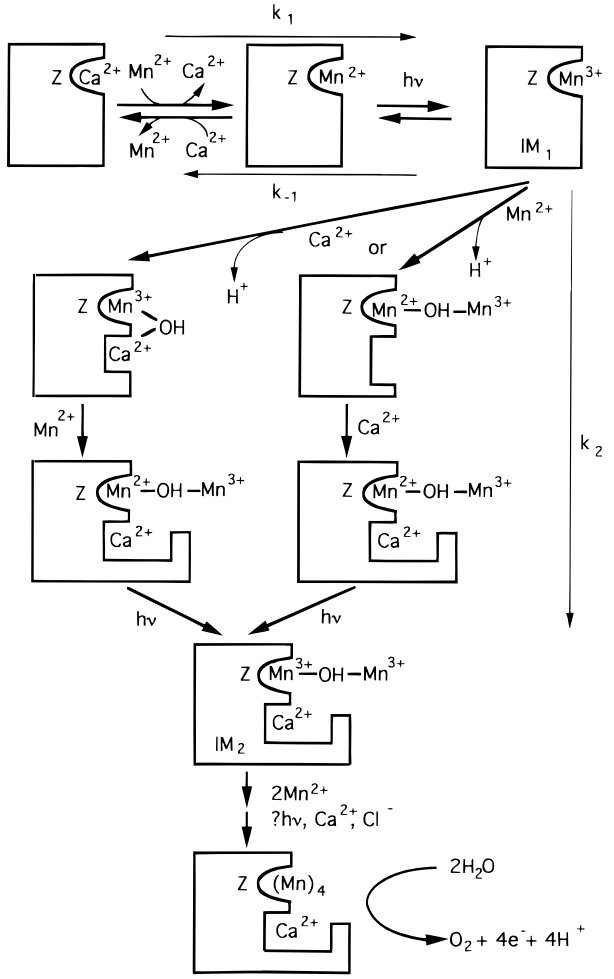

[a] The box represents the apo-PSII complex. The component Z represents Tyr Z, the primary electron acceptor for manganese photooxidation.

calcium to allow efficient utilization of the second photon (the dark k_2 step in Scheme 1) and the decay back to the initial dark state represented by step k_{-1}. Tamura and Cheniae (1987) measured the half-time for decay of an unstable intermediate in photoactivation to be about 1−1.5 s. This intermediate was not directly resolved in their experiments and could only be inferred from the requirement of intermittent light and dark periods. In our work, we directly determined the rate constant for the decay of IM_1 (see Figures 4 and 6) and found that decay is strongly accelerated by calcium. If we interpolate the linear k_{-1} dependence on Ca^{2+} concentration seen in Figure 6 to 50 mM, as was used in the work of Tamura and Cheniae, the half-time for the decay of IM_1 predicted by our results would be equal to 2 s. This agreement of the half-times in both works shows that IM_1 is the first light-induced intermediate in Cheniae's model and IM_2 is the second light-induced intermediate. This comparison of results also clearly indicates that the photoactivation intermediates are basically the same at high (Tamura & Cheniae, 1987) and low (this work) Mn^{2+} concentrations.

Extended Model of Photoactivation. Scheme 2 represents an extended model of photoactivation based on our findings and earlier findings. In the first step of photoactivation, dark binding and light-induced oxidation of the first Mn^{2+} ion occur, forming the apo-PSII-Mn^{3+} species, or IM_1. Accord-

ing to the dependence of k_{-1} on Ca^{2+} concentration (Figure 6), the dark decay of IM_1 involves binding of one Ca^{2+} ion forming a dark species, apo-PSII-Ca^{2+}, as shown in the upper left-hand corner of Scheme 2. The binding site for this Ca^{2+} ion could be the high-affinity Mn^{2+} site or possibly a different site that is strongly coupled to release of manganese from the high-affinity site.

The apparent dissociation constant for Mn^{2+} in the first step of photoactivation is found from our data to be 8 μM at the optimal calcium concentration for photoactivation (8 mM) (see Table 1). This binding constant is close to the binding constant for Mn^{2+} at the high-affinity site, estimated earlier to be 1−10 μM (at lower calcium concentrations) from an analysis of the reduction kinetics of Y_z^+ or DCIP (Hoganson et al., 1989; Blubaugh & Cheniae, 1990; Nixon & Diner, 1992). These results contrast with the Mn dissociation constant measured from its inhibition of electron donation by the exogenous donor DPC, where a value about 10 times smaller is found, 0.15−1.5 μM (Hsu et al., 1987; Ghirardi et al., 1996). The reason for this difference is that the K_i for the DPC electron donation reflects an elementary step of Mn^{2+} binding to the high-affinity site (Ghirardi et al., 1996), while the other assays provide the binding constant for the complex step of Mn^{2+} binding and photooxidation to Mn^{3+}.

As shown in the earlier work**,** proton release can be observed in the first photolytic step of photoactivation (Ananyev & Dismukes, 1996a). This fact is incorporated in Scheme 2 by showing proton release following formation of IM_1. As one possibility, the proton might dissociate from water and form a bridging hydroxide, either between Mn^{3+} and Ca^{2+} or between Mn^{3+} and a second Mn^{2+} ion, as depicted in the two parallel paths in Scheme 2. Accordingly, the pseudo-first-order rate constants in Table 1 apply over a wide range of Mn^{2+} concentrations and so can be converted to bimolecular rate constants by division by the Mn^{2+} concentration (10 μM).

Binding of Ca^{2+} Occurs during the Rate-Determining Step of Photoactivation. As shown in Figure 5, Ca^{2+} specifically stimulates the second step of photoactivation at low concentrations and slows it at higher concentrations due to a nonspecific cation effect. We propose that the requirement for Ca^{2+} for assembly of the tetramanganese cluster, demonstrated in our earlier work, arises from this same calcium assembly site especially in the second step of photoactivation (Ananyev & Dismukes, 1996a,b). The inability to observe the Ca^{2+} requirement for the assembly of the tetramanganese cluster in some earlier works (Miller & Brudvig, 1989; Tamura et al., 1989; Chen et al., 1995) could be due to one or more of the following reasons: (1) the Ca^{2+} concentrations examined were often higher than the K_m for Ca^{2+} binding, (2) the inability to remove Ca^{2+} (and Mn^{2+}) completely which is required for seeing the pre-steady state intermediate, and (3) the inability to separate the competing effects of Ca^{2+} inhibition and stimulation on the rate of photoactivation *vs* the requirement for Ca^{2+} for O_2 evolution in the assembled cluster.

The data in Figure 8 show that the quantum yield of the second photolytic step of photoactivation increases with the dark interval in the range of 3−10 s. This result demonstrates that within the k_2 step the dark process ($IM_1 \rightarrow IM_2$* step in Scheme 1) determines the overall rate of photoactivation. Since this step is both Mn^{2+}- and Ca^{2+}-dependent, we can suggest that several events might be rate-limiting, such as binding of Mn^{2+}, binding of Ca^{2+}, or Ca^{2+}-mediated structural rearrangement of the protein. Out of these events, a slow structural rearrangement has been previously proposed and seems quite probable (Chen et al., 1995; Burnap et al., 1996). As shown in Scheme 2, binding of Ca^{2+} may occur before or after binding of the second Mn^{2+} ion. If Ca^{2+} binds before Mn^{2+}, then the structural rearrangement caused by Ca^{2+} is likely to create a binding site for the second Mn^{2+} ion.

The K_m of 1.4 mM for the Ca^{2+} binding in the second step of photoactivation (see Table 1) falls in the range of the estimated K_m for the low-affinity Ca^{2+} site required for O_2 activity in intact PSII membranes, equal to 1−7 mM (Boussac et al., 1985; Cammarata & Cheniae, 1987; Homann, 1988). This K_m is also exactly the same as the K_m for the Ca^{2+} requirement for reactivation of the steady state oxygen evolution rate by photoactivation in the presence of near-stoichiometric (8 μM) concentrations of Mn^{2+} (Ananyev & Dismukes, 1996a,b). The similarity in these values for the dissociation constants suggests that Ca^{2+} ligation during the second step of photoactivation may occur at the same site required for the expression of oxygen evolution activity in the intact WOC. Since the molecularity for calcium stimulation of the second step of photoactivation is 1 (Figure 5), this leads to the prediction of one calcium ion for expression of oxygen evolution activitiy. According to several studies, there is only one Ca^{2+} binding site in intact PSII membranes, which has different affinities in different S states (Boussac & Rutherford, 1988; Han & Katoh, 1993, 1995; Adelroth et al., 1995). The role of this Ca^{2+} ion in oxygen evolution has been proposed to be a "gatekeeper" to limit the number of substrate water molecules that can access the Mn cluster, on the basis that calcium binding to this site greatly suppresses the accessibility of small molecule reductants to the WOC (Rutherford, 1989; Sivaraja et al., 1989; Tso et al., 1991; Yocum, 1991).

ACKNOWLEDGMENT

We thank Drs. Sergei Khangulov, Noriaki Tamura, and Alexandra Boelrijk and Mr. Daniel Katz for useful discussions and mathematical modeling, respectively.

REFERENCES

Adelroth, P., Lindberg, K., & Andreasson, L.-E. (1995) *Biochemistry 34*, 9021−9027.

Ananyev, G. M., & Dismukes, G. C. (1996a) *Biochemistry 35*, 4102−4109.

Ananyev, G. M., & Dismukes, G. C. (1996b) *Biochemistry 35*, 14608−14617.

Anderson, J. M., Andersson, B. (1988) *Trends Biochem. Sci. 13*, 351−355.

Andreasson, L.-E., Vass, I., & Styring, S. (1995) *Biochim. Biophys. Acta 1230*, 155−164.

Aro, E.-M., Virgin, I., & Andersson, B. (1993) *Biochim. Biophys. Acta 1143*, 113−134.

Berthold, D. A., Babcock, G. T., & Yocum, C. F. (1981) *FEBS Lett. 27*, 231−234.

Blubaugh, D. J., & Cheniae, G. M. (1990) *Biochemistry 29*, 5109−5118.

Blubaugh, D. J., & Cheniae, G. M. (1992) in *Research in Photosynthesis* (Murata, N., Ed.) Vol. II, pp 361−364, Kluwer Academic Publishers,Dordrecht, The Netherlands.

Boussac, A., & Rutherford, A. W. (1988) *Biochemistry 27*, 3476−3483.

Boussac, A., Maison-Peteri, B., Etienne, A.-L., & Vernotte, C. (1985) *Biochim. Biophys. Acta 808*, 231−234.
Burnap, R. L., Qian, M., & Pierce, C. (1996) *Biochemistry 35*, 874−882.
Callahan, F. E., Becker, D. W., & Cheniae, G. M. (1986) *Plant Physiol. 82*, 261−269.
Cammarata, K. V., & Cheniae, G. M. (1987) *Plant Physiol. 84*, 587−595.
Chen, C., Kazimir, J., & Cheniae, G. M. (1995) *Biochemistry 34*, 13511−13526.
Cheniae, G. M., & Martin, I. F. (1966) *Brookhaven Symp. Biol. 19*, 406.
Cheniae, G. M., & Martin, I. F. (1971) *Biochim. Biophys. Acta 253*, 167−181.
Connors, K. A. (1990) *Chemical Kinetics*, VCH Publishers, Inc., New York.
Debus, R. J. (1992) *Biochim. Biophys. Acta 1102*, 269−353.
Ghanotakis, D. F., Babcock, G. T., & Yocum, C. F. (1984) *Biochim. Biophys. Acta 765*, 388−398.
Ghirardi, M. L., Lutton, T. W., & Seibert, M. (1996) *Biochemistry 35*, 1820−1828.
Han, K.-C., & Katoh, S. (1993) *Plant Cell Physiol. 34*, 585−593.
Han, K.-C., & Katoh, S. (1995) *Biochim. Biophys. Acta 1232*, 230−236.
Hoganson, C. W., Ghanotakis, D. F., Babcock, G. T., & Yocum, C. F. (1989) *Photosynth. Res. 22*, 285−293.
Homann, P. H. (1988) *Biochim. Biophys. Acta 934*, 1−13.
Hsu, B.-D., Lee, J.-Y., & Pan, R.-L. (1987) *Biochim. Biophys. Acta 890*, 89−96.
Jegerschold, C., & Styring, S. (1989) in *Current Research in Photosynthesis*(Baltscheffsky, M., Ed.) Vol. II, pp 405−408, Kluwer Academic Publishers,Dordrecht, The Netherlands.
Klimov, V. V., Allakherdiev, S. I., Shuvalov, V. A., & Krasnopolsky, A. A. (1982) *Dokl. Akad. Nauk SSSR 263*, 1001−1007.
Klimov, V. V., Ananyev, G. M., Allakhverdiev, S. I., & Zharmukhamedov, S. K. (1990a) in *Current Research in Photosynthesis*(Baltscheffsky, M., Ed.) Vol. I, pp 247−254, Kluwer Academic Publishers,Dordrecht, The Netherlands.
Klimov, V. V., Shafiev, M. A., & Allakhverdiev, S. I. (1990b) *Photosynth. Res. 23*, 59−65.
Miller, A.-F., & Brudvig, G. (1989) *Biochemistry 28*, 8181−8190.
Miller, A.-F., & Brudvig, G. (1990) *Biochemistry 29*, 1385−1392.
Miyao, M., & Inoue, Y. (1991) *Biochim. Biophys. Acta 1056*, 47−56.
Nixon, P. J., & Diner, B. A. (1992) *Biochemistry 31*, 942−948.
Ono, T.-A., & Inoue, Y. (1983a) *Biochim. Biophys. Acta 723*, 191−201.
Ono, T.-A., & Inoue, Y. (1983b) in *The Oxygen Evolving System of Photosynthesis* (Inoue, Y., et al., Eds,) pp 337−344, Academic Press Japan, Tokyo.
Powels, S. B. (1984) *Annu. Rev. Plant Physiol. 35*, 15−44.
Rutherford, A. W. (1989) *Trends Biochem. Sci. 14*, 227−232.
Segel, I. H. (1975) *Enzyme Kinetics*, John Wiley & Sons, New York, Chichester, Brisbane, and Toronto.
Sivaraja, M., Tso, J., & Dismukes, G. C. (1989) *Biochemistry 28*, 9459−9464.
Tamura, N., & Cheniae, G. M. (1987) *Biochim. Biophys. Acta 890*, 179−194.
Tamura, N., Inoue, Y., & Cheniae, G. M. (1989) *Biochim. Biophys. Acta 976*, 173−181.
Tamura, N., Kamachi, H., Hokari, N., Masumoto, H., & Inoue, H. (1991) *Biochim. Biophys. Acta 1060*, 51−58.
Theg, S. M., Filar, L. J., & Dilley, R. A. (1986) *Biochim. Biophys. Acta 849*, 106−111.
Tso, J., Sivaraja, M., & Dismukes, C. D. (1991) *Biochemistry 30*, 4734−4739.
Vasilikiotis, C., & Melis, A. (1994) *Proc. Natl. Acad. Sci. U.S.A. 91*, 7222−7226.
Yamashita, T., & Tomita, G. (1974) *Plant Cell Physiol. 15*, 69−82.
Yamashita, T., & Ashizawa, A. (1983) in *The Oxygen Evolving System of Photosynthesis* (Inoue, Y., et al., Eds.) pp 327−336, Academic Press Japan, Tokyo.
Yocum, C. F. (1991) *Biochim. Biophys. Acta 1059*, 1−15.

BI970187F